The relationship between the aspect ratio and multi-physical fields in aluminium reduction cells

by H. Zhang*, J. Li*, Y. Lai*, W. Liu*, Y. Xu*, Z. Wang*, and X. Zhang*

Synopsis

The relationship between the aspect ratio and physical fields in aluminium reduction cells wase studied numerically. The aspect ratio was firstly defined and 7 kinds of 320 kA cells with different aspect ratios were put forward. By using numerical simulation, the relationship between the aspect ratio and the electric-magnetic flow fields, magnetohydrodynamic stabilities, and thermal stability was discussed. It is concluded that the electric-magnetic flow field distributions are greatly affected by the aspect ratio. From the perspective of magnetohydrodynamics stability, the larger the aspect ratio is, the more stable the cell will be. A larger aspect ratio is more beneficial for the thermal stability under the same current density.

Keywords

aluminium, electrolysis, aspect ratio, electric-magnetic flow fields, magnetohydrodynamics, thermal stability.

Introduction

Spatial dimension is one of the key parameters in aluminium reduction cells. It not only determines the distributions of multi-physical fields, such as electric-magnetic flow fields, magnetohydrodynamic (MHD) stability, and thermal stability, but also influences the cell structure and operation technology. Compared with the cell height, the cell length and width are more important, because they closely relate to the current density and also determine the economic and technical characteristics of the cell.

In the 1990s, the effects of aspect ratio (length width ratio) had been mentioned by researchers, but not studied as a key point. Sneyd[1] studied the stabilities of aluminium reduction cells by means of mode-coupling. His results indicated that an aspect ratio of about 7.7/3.0 maximizes frequency separation, but not all potential resonances actually lead to instability. Ziegler[2] studied the relationship between the instabilities of K-H (Kelvin-Helmholtz) and critical velocity, and found that the critical velocity was greatly influenced by the cell length and width. However, in this investigation, the cell length and width were

set at 11.30 m and 3.08 m respectively, which mean that there were no discussions about the relationship between the aspect ratio and critical velocity. More recently in China, Yao[3] studied the instabilities of the GY320 cell and pointed out that the aspect ratio of the GY320 was 4.33, which is smaller than that of Pechiney AP-30 but larger than that of the 400 and 500 kA cell designed by Dupuis, and the cells would be more stable if the anode in GY320 was modified to 1.60 m × 0.80 m. In a word, the aspect ratio is an important parameter in an aluminium reduction cells but little research work has been done to date.

The spatial structure of the reduction cell is very complex. Altering the aspect ratio will lead to a change in the cell structure and eventually a change in physical fields. Using currently available techniques for modelling multi-physical fields in reduction cells, it is very difficult to construct cell models that can incorporate significant structural changes. This is why there are very few investigations of aspect ratio. Fortunately, in our research group, a fast modelling method has been established for constructing multi-physical fields simulation models, which could be used to study the effect of aspect ratio on physical fields in aluminium reduction cells.

The objective of this investigation was to study the relationship between the aspect ratio and physical fields numerically. In this paper, the definition of aspect ratio is given firstly, and then seven cells with different aspect ratios are designed. The relationship between the aspect ratio and electric-magnetic flow fields, MHD stabilities, and thermal stabilities is then discussed.

* School of Metallurgical Science and Engineering, Central South University, Changsha, China.

The relationship between the aspect ratio and multi-physical fields

Definition of aspect ratio and the research scheme

The aspect ratio (AR) of an aluminium reduction cell can be defined as:

$$AR = \frac{L}{W} \qquad [1]$$

$$L = w_a \times n + g_a \times (n-1) \qquad [2]$$

$$W = l_a \times 2 + g_c \qquad [3]$$

where w_a is the width of the anode, g_a is the inter-anode channels width, n is half of the total anode number, l_a is the length of the anode, and g_c is the centre channel width.

Table I lists the structure parameters of several types of prebaked cell technologies being used in the aluminum industry. For 300 kA cells, the current densities are between 0.73~0.82 A·cm-2, and the AR between 3.96~4.26; while for 320 kA cells, the parameters are 0.70~0.84 A·cm-2 and 3.56~5.44 respectively, 0.71 A·cm-2 and 5 for 350 kA cells; and 0.82 A·cm-2 and 4.02 respectively for 400 kA prototype cells. This indicates that there are dramatic differences in spatial structure for different cell types. Obviously, the AR of cells will affect the electric-magnetic flow fields, the MHD instabilities, and thermal equilibrium. The relationships between AR and multi-physical fields need to be discussed.

In this article, we construct models of 320 kA cells with different ARs. In order to ensure that AR is the only variable,

the influences of AR on physical fields were analysed under the same current density and other technological parameters.

The detailed structure parameters of the seven designed cells are shown in Table II. The relationship studied in this article include the following:

➤ Distribution of electric-magnetic flow field in a 320 kA with AR changed from 3.2 to 5.4 cell at a current density of 0.71 A·cm-2.
➤ MHD stabilities for all the cells in Table II.
➤ Qualitative analysis of thermal stabilities.

Since there are various kinds of busbar configuration for each cell and the difference between them can be significant, two problems will appear when considering the busbar in this paper. Firstly, it is difficult to decide which busbar configuration is the optimal; secondly, building the busbar model it is time-consuming. In comparison, the distributions of electric-magnetic flow fields caused by the internal conductors are more analogous and easier to model with good comparability. Therefore, in this article, the influences of busbar configurations are not included.

The multi-physical field modelling scheme is shown in Figure 1. The electric-magnetic models were developed with ANSYS by using the parametric design language, the computational domains were discretized by millions of eight-node hexahedral elements, and then the electric-magnetic fields were resolved using the finite element method. Multi-phase flow models were established with CFX by introducing

---

Table I

Structure parameters of several types of prebaked cell technologies[3–7]

	Marc-400	Alcoa-817	AP-30	VAW-300	SY-350	GY-320	GP-320	QY-300
Amperage, kA	400	320	320	300	350	320	320	300
Current density (ρ), (A·cm-2)	0.817	0.843	0.821	0.732	0.707	0.714	0.697	0.733
Number of anodes	36	32	40	32	24	40	48	40
Length of anodes, m	1.700	1.625	1.500	1.600	1.550	1.600	1.450	1.550
Width of anodes, m	0.800	0.730	0.650	0.800	1.330	0.700	0.660	0.660
Interanode channels width, mm	40	28	40	40	40	40	40	40
Centre channel width, mm	350	150	80	180	180	180	180	180
Length of cell (L), m	15.080	12.100	13.760	13.400	16.400	14.760	16.760	13.960
Width of cell (W), m	3.750	3.400	3.080	3.380	3.280	3.380	3.080	3.280
Aspect ratio	4.02	3.56	4.46	3.96	5	4.36	5.44	4.256

Table II

Structure parameters of designed prebaked cell technologies (I=320 kA)

	AAR1	AAR2	AAR3	AAR4	AAR5	AAR6	AAR7
Current density, A·cm-2	0.714	0.714	0.714	0.714	0.714	0.714	0.714
Number of anodes	32	36	40	40	40	44	48
Length of anodes, m	1.868	1.776	1.620	1.600	1.580	1.570	1.430
Width of anodes, m	0.750	0.700	0.691	0.700	0.709	0.648	0.650
Interanode channels width, mm	40	40	40	40	40	40	40
Center channel width, mm	180	180	180	180	180	180	180
Number of cathodes	21	23	27	27	27	27	31
Length of cathodes, m	0.565	0.540	0.515	0.515	0.517	0.525	0.505
Width of cathodes, m	3.956	3.772	3.460	3.420	3.380	3.360	3.080
Intercathode channels width, mm	39	41	28	35	40	37	30
Anode side distance, mm	280	280	280	280	280	280	280
Anode end distance, mm	390	390	390	390	390	390	390
Length of cell, m	12.600	13.280	14.580	14.760	14.940	15.096	16.520
Width of cell, m	3.916	3.732	3.420	3.380	3.340	3.320	3.040
Aspect ratio (AR)	3.22	3.56	4.26	4.37	4.47	4.55	5.43

The relationship between the aspect ratio and multi-physical fields
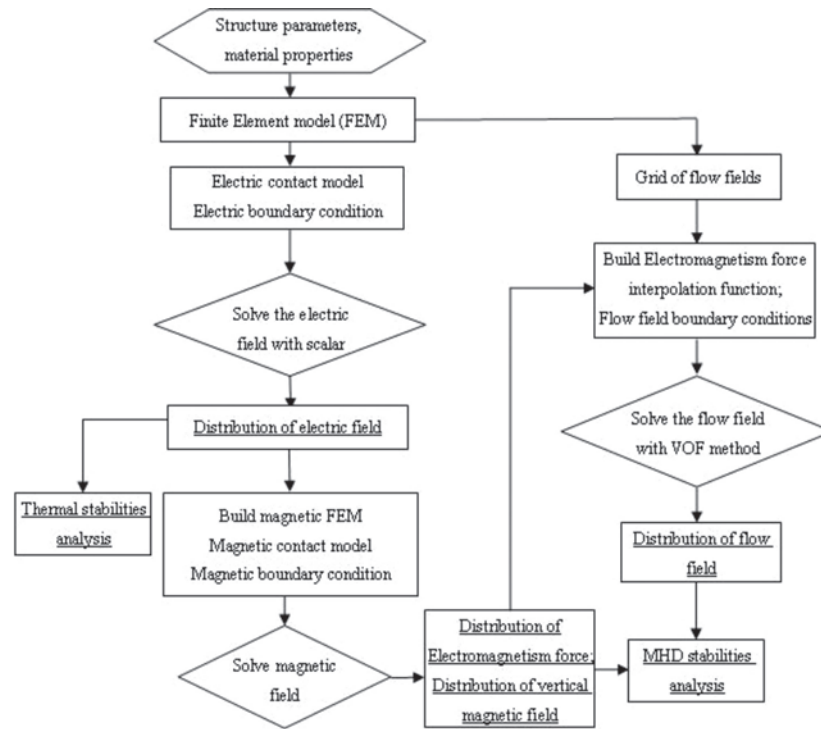
Figure 1—Flow chart of the research scheme

the electric-magnetic forces which were predicted by the electric-magnetic computation, and the flow fields were resolved using the finite volume method based on the SIMPLEC algorithm. The MHD stability equations are basically consistent with those developed by Urata[8,9], Bojarevics[10] and Droste[11], while in the solutions with a Fourier expansion method, the surface fitting functions based on the least-square method were built to introduce discrete electric-magnetic results calculated with ANSYS. The detailed methods in multi-physical fields modelling designed by our research group can be found in[12–14], and a 3D geometry modelling of the reduction cell corner used in the models is presented in Figure 2.

Relationship between the AR and multi-physical field distributions

Electric field distributions

When $I = 320$ kA and $\rho = 0.714$ A·cm^{-2}, the voltage of the system, anode, and cathode under different ARs is shown in Figure 3, which indicates that the anode, cathode, and system voltage drops decrease with increasing AR.

Magnetic field distributions

Figure 4 shows the magnetic field component of the cells with different ARs. It can be seen that the magnetic field component and total magnetic field decrease with increasing AR under constant current density.

Flow field distributions

Figure 5 shows the horizontal velocity vector distributions in the metal pads of AAR1, AAR2, AAR4, and AAR7 cells. It

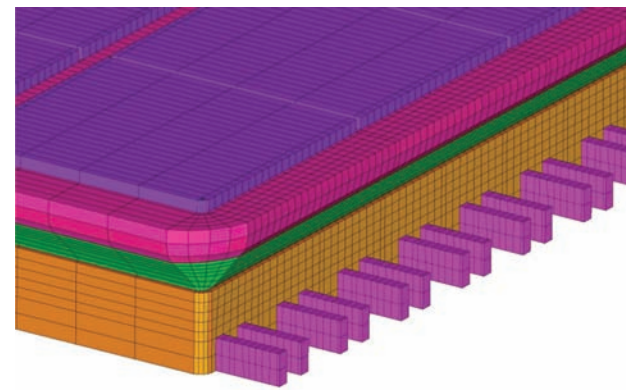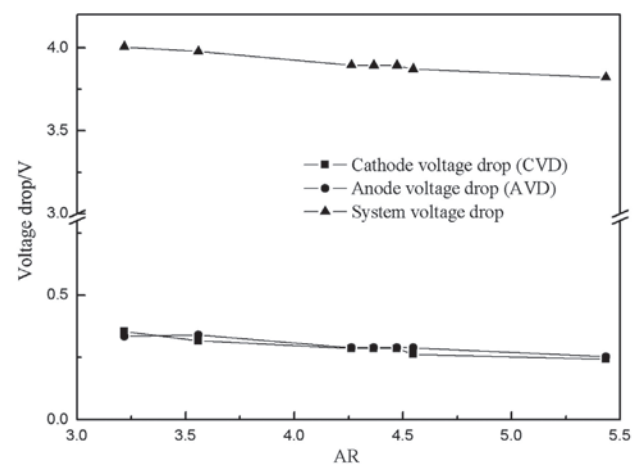Figure 2—3D modeling of the reduction cell corner

Figure 3—Voltage drop versus AR with $I = 320$ kA and $\rho = 0.714$ A·cm^{-2}
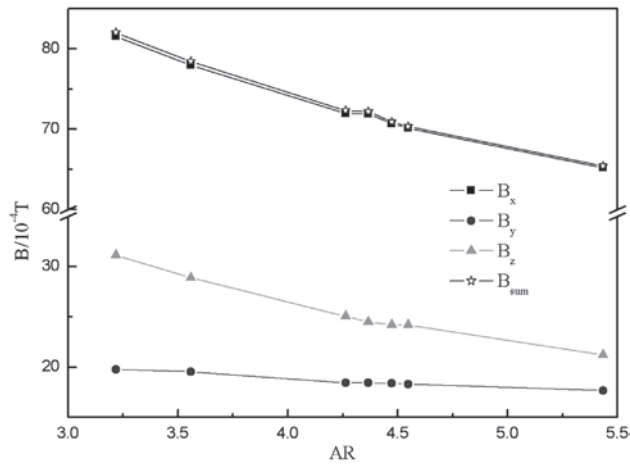
Figure 4—Maxmium magnetic field value versus AR with I = 320 kA and ρ = 0.714 A·cm^{-2}

Figure 5—Velocity field in aluminum layer, (a) AAR1 (V_{max} = 13.11 cm·s^{-1}, V_{avg} = 3.04 cm·s^{-1}), (b) AAR2 (V_{max} = 11.31 cm·s^{-1}, V_{avg} = 2.39 cm·s^{-1}), (c) AAR4 (V_{max} = 9.76 cm·s^{-1}, V_{avg} = 1.94 cm·s^{-1}), (d) AAR7 (V_{max} = 6.16 cm·s-1, V_{avg} = 1.12 cm·s^{-1})

can be seen that there are four vortices in the metal pad under symmetrical electric-magnetic forces, and the velocity in the middle is smaller than in the end and tape areas. The maximum velocities in AAR1, AAR2, AAR4, and AAR7 cells are 13.11 cm·s-1, 11.31 cm·s-1, 9.76 cm·s-1, and 6.16 cm·s-1 respectively, and the average velocities are 3.04 cm·s-1, 2.39 cm·s-1, 1.94 cm·s-1, and 1.12 cm·s-1 respectively, which means that the velocity is decreasing with increasing AR, as shown in Figure 6.

According to the electric-magnetic field results from our models, when the AR increased, the horizontal current density will decrease and the vertical current density will increase by almost the same amplitude; therefore the horizontal electric-magnetic force, which is the main driving force of the aluminium, electrolysis will also decrease since the horizontal magnetic field is much larger than the vertical. As a result, the peak and average velocities will decrease.

MHD instabilities

Using the surface-fitting method, the vertical magnetic field component was transformed from a discrete value and resolved with ANSYS to a continuous function that would be used in MHD instability analysis based on a Fourier expansion method.

Figure 7 show the oscillation spectrograms of the seven cells. It can be seen that the oscillation stabilities improve as the AR increases. One of the reasonable explanations is that the vertical magnetic field is smaller for cells with a larger AR, although the magnetic fields distribution is similar for all the cells studied in this paper.

In Figure 7(a), the red triangle symbol at y=0 represents the natural frequencies of the gravity wave, which indicates that the oscillations caused by gravity wave are quite stable.

Thermal stabilities

Beran[15] proposed the following equation to calculate the heat loss per unit current:
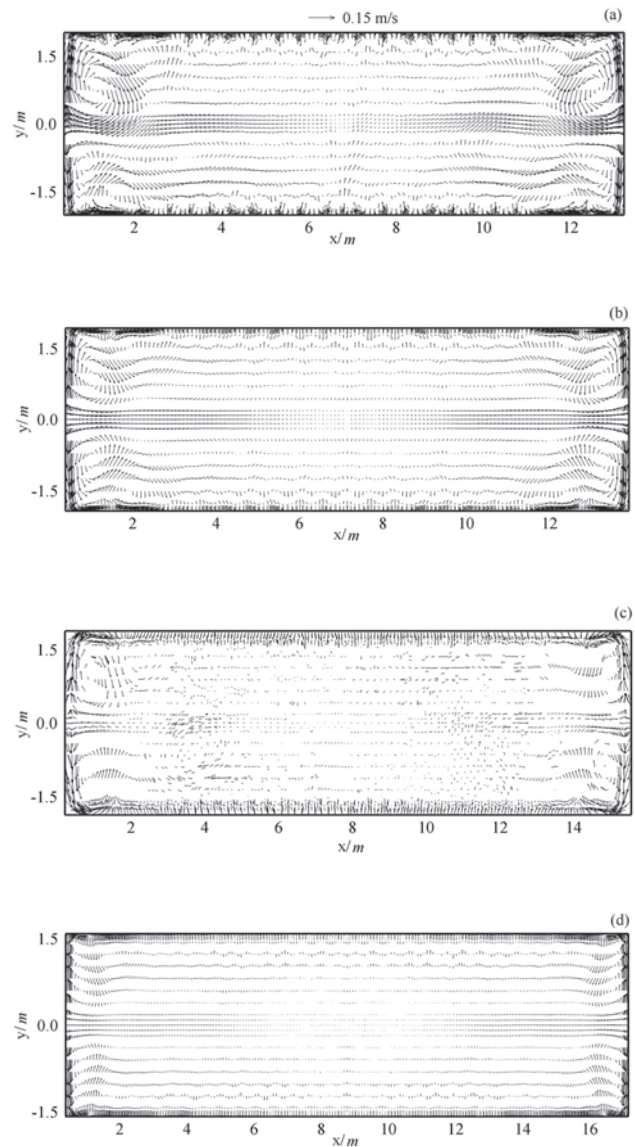
$$Q / I = V_{sys} - 1.649\eta - 0.48 \qquad [4]$$
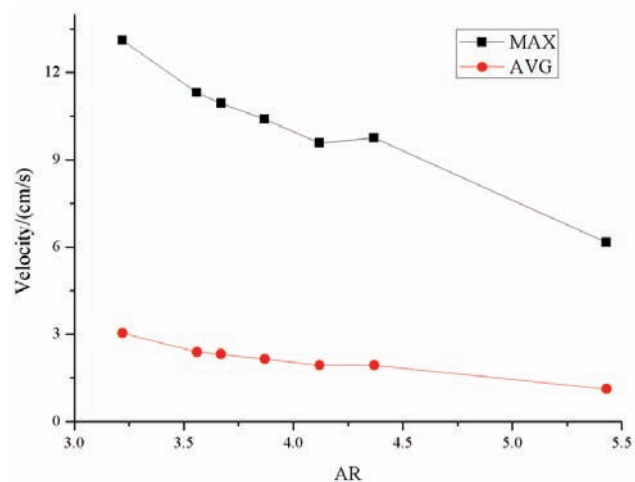
Figure 6—Velocity versus AR

The relationship between the aspect ratio and multi-physical fields

where V_{sys} is the system voltage and η is the current efficiency. It indicates that as long as the current efficiency and system voltage stay the same, the heat loss is a constant for all cells even when the capacity of the cell varies.

Increasing the AR can enlarge the surface area of cells. Figure 8 shows the heat loss intensity per unit area for different ARs. It suggests that the bigger the AR is, the lower the heat loss intensity is, and consequently the lower the sidewall temperature will be, which is beneficial for the formation of the ledge.
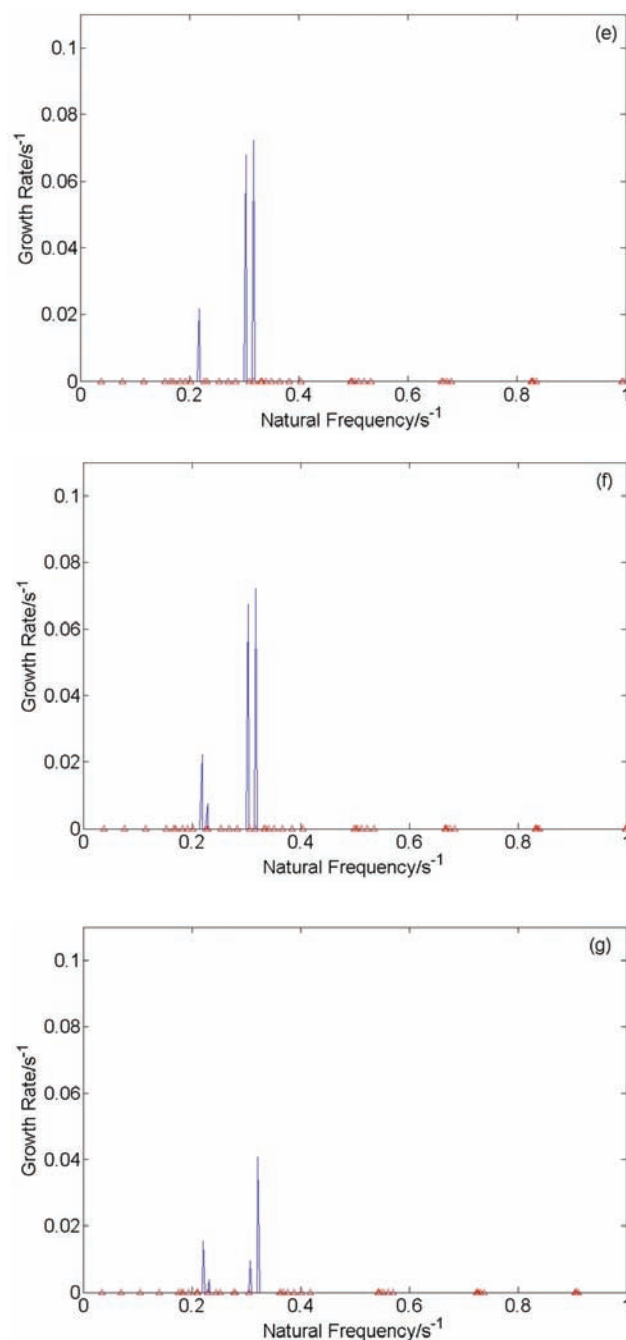

Figure 7—Oscillation spectrograms, (a) AAR1, (b) AAR2, (c) AAR3, (d) AAR4

Figure 7 (continued)—Oscillation spectrograms, (e) AAR5, (f) AAR6, (g) AAR7

The relationship between the aspect ratio and multi-physical fields
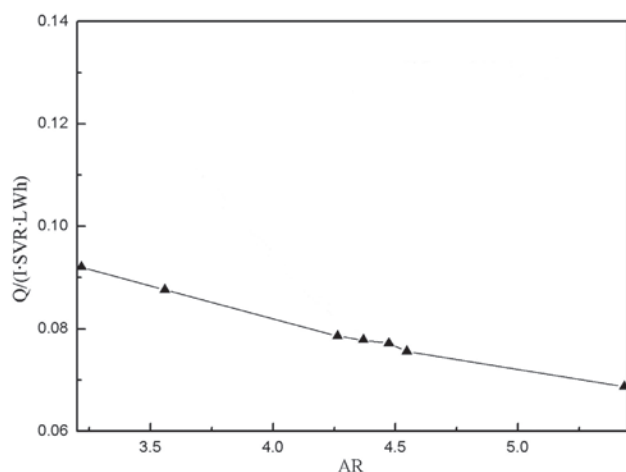

Figure 8—Heat loss intensity per unit area versus AR

Conclusions

This paper studies the relationship between the AR and the multi-physical fields in aluminium reduction cells. The definition of AR definition was first presented, and seven different 320 kA cells were then designed. The relationships between the AR and the electric-magnetic flow fields, MHD stabilities, and thermal stabilities were discussed. The following conclusions can be drawn:

➤ Under the same current intensity and density, the system, anode, and cathode voltages decrease with increasing AR

➤ The flow field appear to consist of four vortices in the metal pad, and the velocity in the middle is smaller than that in the end and in the four vortices corner. The velocity in the metal pad decreases with increasing of AR

➤ The analysis of MHD stabilities indicates that the cell become more stable as the AR increases, the reason for this being that the vertical magnetic field is smaller for cells with bigger ARs

➤ The discussion of thermal stabilities shows that, under the same current density, the thermal stabilities can be improved when the AR increases.

Acknowledgements

References

1. SNEYD, A.D. and WANG, A. Interfacial instability due to MHD mode coupling in aluminum reduction cells. *Journal of Fluid Mechanics*, vol. 263, 1994. pp. 343–359.

2. ZIEGLER, D.P. Stability of metal/electrolyte interface in Hall-Héroult cells: effect of the steady velocity. *Metallurgical Transactions B*, vol. 24B, 1993. pp. 899–906.

3. YAO, S.H. The application of aluminium reduction theories and axperiences to high amerage pots [EB/OL]. http://www.gami.com.cn, 2007.

4. MARC, D. Thermo-electric design of a 400 kA cell using mathematical models: A tutorial. *Light Metals: Proceedings of Sessions, TMS Annual Meeting, Warrendale, Pennsylvania*, 2000. pp. 297–302.

5. TABEREAUX, A. Prebake cell technology: *A Global Review[J].JOM*, vol. 52. 2000. pp. 22–28.

6. REVERDY, M., HOMSI, P., and JOLAS, J.M. AP 30 pot technology and experience gained from the recently started potlines. *Light Metals: Proceedings of Sessions*, *TMS Annual Meeting*, Warrendale, Pennsylvania, 1995. pp. 405–411.

7. YIN, E.S., LIU, Y.G., XI, C.M., and ZHANG, J.Z. Developing the GP-320 cell technology in China, *Light Metals*, 2001. pp. 213–218.

8. Urata, N. Magnetics and metal pad instability. *Light Metals 1985*. Metallurgical Society of AIME, New York, NY: 1985. pp. 581–591.

9. URATA, N. Wave mode coupling and instability in the internal wave in aluminum reduction cells. Kvande, H. (ed.). *Light Metals 2005*. San Francisco, CA: The Minerals, Metals and Materials Society, 2005. pp. 455–460.

10. BOJARVICS, V. and V.ROMERIO, M. Long waves instability of liquid metal-electrolyte interface in aluminum electrolysis cells: A generalization of Sele's criteria. *European Journal of Mechanics B*, vol. 13, 1994. pp. 33–56.

11. DROSTE, C., SEGATZ, M., and VOGELSANG, D. Improved 2-dimensional model for magnetohydrodynamic stability analysis in reduction cells. Light Metals 1998. San Antonio, TX: The Minerals, Metals and Materials Society, 1998. pp. 419–428.

12. LI, J., LIU, W., and LAI, Y.Q. Improved finite element model for electro-magnetic analysis in aluminum cells. *JOM*, vol. 60. 2008. pp. 58–61.

13. LI, J., LIU, W., and LAI, Y.Q. Coupled simulation of 3D electro-magneto-flow field in Hall-Héroult cells using finite element method, *Acta Metallurgica Sinica* (English Letters), vol. 19, 2006. pp. 105–116.

14. LI, J., XU, Y., ZHANG, H., and LAI, Y. An inhomogeneous three-phase model for the flow in aluminium reduction cells. *International Journal of Multiphase Flow*, vol. 37, 2011. pp. 46–54.

15. BERAN, P., VON, K.R., and LANGE, H.P. Impact of current increase on specific energy consumption. Light Metals 2001. New Orleans, LA. The Minerals, Metals and Materials Society, 2001. pp.179–184.   ◆